### Title
A disinhibitory microcircuit initiates critical-period plasticity in the visual cortex.




### Journal
Nature, 501(7468)

### ISSN
0028-0836



### Authors
Kuhlman, Sandra J
Olivas, Nicholas D
Tring, Elaine
et al.



### Publication Date
2013-09-01

### DOI
10.1038/nature12485

Peer reviewed

HHS Public Access

Author manuscript

*Nature*. Author manuscript; available in PMC 2014 March 26.

Published in final edited form as:

*Nature*. 2013 September 26; 501(7468): 543–546. doi:10.1038/nature12485.

# A disinhibitory microcircuit initiates critical period plasticity in visual cortex

**Sandra J. Kuhlman**[1,4,5], **Nicholas D. Olivas**[2,4], **Elaine Tring**[1], **Taruna Ikrar**[2], **Xiangmin Xu**[2,3], and **Joshua T. Trachtenberg**[1]

[1]Department of Neurobiology, David Geffen School of Medicine, University of California, Los Angeles

[2]Department of Anatomy and Neurobiology, University of California, Irvine

[3]Department of Biomedical Engineering, University of California, Irvine

## Abstract

Early sensory experience instructs the maturation of neural circuitry in cortex [1,2]. This has been extensively studied in the primary visual cortex where loss of vision to one eye permanently degrades cortical responsiveness to that eye [3,4], a phenomenon known as ocular dominance plasticity (ODP). Cortical inhibition mediates this process [4-6], but the precise role of specific classes of inhibitory neurons in ODP is controversial. Here we report that evoked firing rates of binocular excitatory neurons in primary visual cortex immediately drop by half when vision is restricted to one eye, but gradually return to normal over the following 24 hours, despite the fact that vision remains restricted to one eye. This restoration of binocular-like excitatory firing rates following monocular deprivation results from a rapid, though transient reduction in the firing rates of fast-spiking, parvalbumin-positive (PV) interneurons, which in turn can be attributed to a decrease in local excitatory circuit input onto PV interneurons. This reduction in PV cell evoked responses following monocular lid suture is restricted to the critical period for ODP and appears to be necessary for subsequent shifts in excitatory ODP. Pharmacologically enhancing inhibition at the time of sight deprivation blocks ODP and, conversely, pharmaco-genetic reduction of PV cell firing rates can extend the critical period for ODP. These findings define the microcircuit changes initiating competitive plasticity during critical periods of cortical development. Moreover, they show that the restoration of evoked firing rates of L2/3 pyramidal neurons by PV-specific disinhibition is a key step in the progression of ocular dominance plasticity.

Throughout the neocortex, form and function of neural circuitry are shaped by experience [1,2,7,8]. This sensitivity to experience is most pronounced during adolescence, and



[4]These authors contributed equally to this work.

[5]Present address: Department of Biological Sciences and the Center for the Neural Basis of Cognition, Carnegie Mellon University, Pittsburgh

**Author contributions:**

SK&ET performed the *in vivo* awake and anesthetized recordings. SK performed the diazepam/OGB-1 experiments. ET performed the DREADD/GCamp6 experiments. NO and TI performed the glutamate uncaging experiments. XI oversaw the glutamate uncaging experiments. JT oversaw all aspects of the project. SK, NO, XX and JT wrote the manuscript and prepared the figures.

has been most extensively studied in the primary visual cortex [3,9], where occluding vision through one eye (monocular deprivation; MD) results in cortical blindness to this eye, even after normal vision is restored [3,10-12]. With the goal of identifying the initial changes in cortical function following MD we used loose-cell attached recordings to isolate visually evoked responses from single neurons in binocular visual cortex in alert mice (Fig. 1a).

Unexpectedly, we found that visually evoked responses of excitatory pyramidal neurons (PYR) in L2/3 one day after contralateral MD were roughly twice as strong as those in control mice. Evoked firing rates to stimulation through the ipsilateral eye, which had not been deprived, were approximately 2-fold higher than in controls (Fig. 1b,c; MD=2.9±0.4Hz, Control=1.5±0.4Hz one-way ANOVA P= 0.028, followed by post-hoc comparison, Tamhane corrected P value, P=0.046). Indeed, firing rates evoked by monocular viewing through the open eye after 1d MD were sufficiently elevated that they were indistinguishable from firing rates evoked during binocular viewing conditions in controls (Fig. 1b,c; Binocular=3.5±0.6Hz, Tamhane corrected P=0.834). A doubling in excitatory firing rates was also seen when we acutely re-opened the deprived contralateral eye and recorded responses to visual stimulation while shuttering the ipsilateral eye (Fig. 1b,c; MD=4.8±0.7Hz, Control=2.4±0.4Hz, Mann-Whitney U P=0.02). Notably, neurons were not responsive to stimulation through the sutured contralateral eye in alert mice. These findings show that following an immediate drop in visually evoked firing rates after MD (because responses are now only driven through one eye), evoked firing rates of PYR neurons are restored as cortical responsiveness to vision through the open eye increases. Thus, after 1 day of MD the firing rates of PYR neurons in L2/3 of binocular visual cortex in alert mice that are viewing a scene with only one eye are roughly equivalent to firing rates in normal mice viewing a scene with both eyes.

The increased responsiveness of L2/3 PYR neurons may result from an increase of excitatory drive onto these neurons, enhanced intrinsic excitability, a reduction of inhibitory drive onto these cells, or any combination of these. To examine the possibility that excitatory drive onto L2/3 PYR neurons increases after MD, we assayed the connectivity strength and laminar distribution of presynaptic excitatory inputs onto L2/3 PYR neurons in binocular cortex in acute brain slices using laser scanning photo stimulation (LSPS) via glutamate uncaging [13] (Fig. 1d-f; Fig. S1). In control mice, maps of excitatory laminar inputs to L2/3 PYR neurons were consistent with those shown in prior published studies [13,14], with most inputs from L4, L5a and L2/3 as well as some weak input from deeper layers (Fig. 1e,f). MD did not significantly alter the amplitudes of excitatory postsynaptic currents (EPSCs) resulting from stimulation of presynaptic neurons originating in any cortical layer (two-way ANOVA on ranks P= 0.756; Fig. 1e,f), indicating that excitatory inputs to L2/3 pyramidal neurons were not altered at this early stage of plasticity. Spatially restricted photostimulation activates between 50 and 100 neurons at each LSPS location [15], though most of these stimulated neurons are not connected to the neuron being recorded. Because of this, glutamate uncaging may also be used to measure aggregate excitatory synaptic input onto the target neuron by evaluating the number of EPSCs elicited per LSPS location; this measure was also not different between control and 1d MD (Fig. S1). Taken together, local circuit mapping data indicate that 1 day of MD does not significantly change the strength or number of excitatory inputs to L2/3 PYR neurons from

any cortical layer. Consistent with a previous report [16], we also did not find any evidence for a significant change in intrinsic excitability of the L2/3 PYR neurons whose inputs we mapped (Fig. S1g), nor did we find evidenced for a change in resting membrane potential (Control: -67.46±1.5mV, n=8 cells from 3 animals; MD -65.9±1.4mV, n=7 cells from 4 animals; Mann-Whitney U P= 0.73).

A remaining possibility is that a decrease in local inhibition underlies the enhanced visual responsiveness of L2/3 PYR neurons we observe after MD. Fast-spiking, parvalbumin-positive basket inhibitory neurons, referred to as PV cells, are increasingly implicated in both critical period and adult plasticity [5,17]. To measure the impact of 1d MD on PV responses, we used *in vivo* two-photon imaging to target cell-attached recordings to PV cells expressing the red fluorescent protein tdTomato. Spike waveform analysis was used to verify the identity of recorded neurons (Fig. 2a); recordings were made in alert and urethane-anesthetized mice. Notably, the effect of 1d MD on evoked firing rates of PV cells was opposite of what we found for PYR neurons – whereas PYR spike rates roughly doubled, PV spike rates were roughly reduced by half. In anesthetized mice, responses to stimulation through the ipsilateral, open eye were reduced by 42% (Fig. 2b,c ; Control: 16.2±2.0Hz, MD: 9.5±0.9 Hz; two-way repeated measures ANOVA taking into account the pairwise relationship between ipsilateral and contralateral eye responses recorded for the same cell P=0.002, followed by post-hoc comparison, Bonferroni-corrected P=0.02), and responses to stimulation through the re-opened deprived, contralateral eye were also reduced, in this case by 54% (Control: 19.8±2.4Hz, MD: 9.2±0.9Hz; Bonferroni-corrected P=0.002). Similarly, in alert mice, PV responses to stimulation through the open eye dropped by 58% relative to controls after 1d MD (Control: 14.8±3.1Hz, n=10 cells from 8 animals; MD: 6.2±0.9Hz, n=10 cells from 7 animals; Mann-Whitney U P=0.001). These recordings show that MD induces a rapid and severe drop in PV cell firing rates. Importantly, this effect is present for both eyes – responses through either the open or formerly closed eye were reduced by roughly half.

To identify the cause of this rapid, binocular reduction in visually evoked firing rates of PV cells, we again turned to recordings in acute brain slices to measure intrinsic excitability and to map the connectivity strength and laminar position of presynaptic excitatory inputs to PV cells. PV cells expressing tdTomato were visually targeted, their fast-spiking firing patterns were confirmed, and these cells were filled with biocytin for post-hoc morphological analysis. We found no evidence for altered intrinsic excitability as a function of current injection after MD (Fig. S2), nor did we detect a change in resting membrane potential (Control: -65.4±1.5 mV, n= 7 cells from 3 animals; MD: -64.1±0.74 mV, n= 7 cells from 4 animals; Mann-Whitney U P>0.8). However, glutamate uncaging revealed a ~70% reduction in excitatory drive from cortical layers 4 and upper layer 5 onto L2/3 PV cells after 1d MD (Fig. 3). The frequency of evoked (Fig. 3b) and spontaneous (Fig. 3c,d) EPSCs were significantly reduced in PV cells after 1d MD, while the amplitude of spontaneous EPSCs was unchanged (Fig. 3e), suggesting both a weakening and reduction of excitatory synaptic inputs onto PV cells occurring at these earliest stages of cortical plasticity.

Notably, the rapid binocular reduction of PV firing rates after MD is transient. When MD was extended to 3 days, PV responses to stimulation of the deprived, contralateral eye

(measured after acutely opening the sutured lids) remained as weak as they were after 1d MD, but the strength of PV responses evoked by ipsilateral eye stimulation returned to normal (Fig. S3). Thus, the rapid, reduction in PV spike rates after 1d MD is soon replaced by a restoration of normal PV responses to ipsilateral eye stimulation, which shifts PV ocular dominance toward the open eye.

A major question emerging from these findings is whether the transient binocular disinhibition following lid suture is necessary for subsequent shifts in excitatory ocular dominance. If so, one prediction is that maintaining inhibition after MD will prevent excitatory plasticity. To examine this we enhanced inhibition by injecting the use-dependent GABA-A agonist, diazepam (DZ), into the ventricles of P28 mice immediately after suturing the contralateral eye. Diazepam treatment effectively prevented the increase in ipsilateral eye excitatory firing rates seen after 1d MD, but did not silence evoked activity (Fig S4a,b).

Mice were exposed to 3 days of MD, and received intraventricular injections of either saline or DZ for the first two days. Cortical ocular dominance was assayed 3 days after MD by imaging visually evoked fluorescent changes in L2/3 neurons bulk loaded with the calcium indicator Oregon Green BAPTA-1. Consistent with a role for disinhibition in ocular dominance plasticity, intraventricular diazepam (DZ), but not vehicle, prevented shifts in cortical ocularity following MD (Fig S4c-h).

Since ocular dominance plasticity is restricted to the critical period [9], a second prediction is that MD will not alter PV firing rates when performed thereafter. Supporting this we found no significant changes in evoked PV firing rates in monocularly-deprived adult mice (age P42-45), relative to age-matched controls (Fig. S5).

A third prediction is that ODP will be enhanced in older mice if PV spike rates are artificially reduced after MD. There is some precedent for this view [18]. In order to manipulate PV spike rates *in vivo*, we expressed hM4D inactivating Gi-coupled DREADD receptors [19-22] selectively in PV cells. Binding of the ligand clozapine-N-oxide (CNO) to hM4D receptors activates G-protein inwardly rectifying potassium channels, thereby reducing spike rates in target neurons for 9-12 hours [23] (Fig. S6). Three days of MD beginning at P35 does not normally shift cortical ocular dominance [9]. To determine whether a transient reduction in PV-mediated inhibition could reveal ODP in mice of this age, we tracked changes in cortical ocular dominance by imaging cortical responses to ipsilateral and contralateral eye stimulation longitudinally in mice expressing the genetically encoded calcium indicator GCaMP6 [24] in layer 2/3 of binocular visual cortex. P35 mice given 2 injections of CNO at 12-hour intervals immediately after lid suture (1 day of reduced PV inhibition) showed significant decreases in cortical responsiveness to the deprived eye without any significant change in open, ipsilateral eye responses, whereas age-matched controls receiving similar injections of saline showed no changes in either measure (Fig. 4). Thus, a 24-hour period of diminished PV firing is sufficient to restore juvenile-like ocular dominance plasticity after the closure of the critical period.

The shift in ocular dominance following eye closure has been a long-standing paradigm for studying cortical plasticity. Mounting evidence implicates PV inhibitory neurons as regulators of this plasticity. How they do so, however, has remained incompletely understood. The data we present here define the role of PV cells in this process, by showing that MD results in a rapid, but transient reduction in PV-based inhibition, which restores PYR firing rates to pre-deprivation levels. Without this restoration of normal excitatory firing rates, subsequent competitive plasticity will not occur.

Our data and earlier papers examining the plasticity of the GABA population as a whole [25,26] or specifically PV cells [27] report that inhibitory responses ultimately shift towards the open eye after MD. Furthermore, there is a consensus that in non-deprived conditions, inhibitory cells are more binocular than excitatory cells in mice with normal GABA levels [25,27]. However, our data differ significantly from earlier studies on two fundamental issues: 1) the rate and direction of PV cell plasticity, and 2) the role of PV cell plasticity in excitatory ODP. Specifically, the possibility that PV cells become transiently, and paradoxically more responsive to deprived eye stimulation, thereby suppressing deprived-eye responses of excitatory neurons and shifting excitatory ocular dominance towards the open eye, was raised in a study that measured the ratio of the contralateral and ipsilateral eye responses in PV cells after brief MD [27]. In our measures of PV spike rates we did not find this paradoxical shift. Instead, we found that a rapid, transient, and binocular reduction of fast-spiking inhibition permits, but does not instruct synaptic competition among excitatory neurons. Our data redefine the role of fast-spiking inhibitory neurons as gating excitatory plasticity. It is the reduction of inhibition and the restoration of normal excitatory spike rates that permits competitive ocular dominance plasticity to proceed based on the relative strengths of the two eye's inputs.

Distinct mechanisms govern the influence of sensory experience on cortical plasticity early in life, in the form of passive sensory exposure, and in adulthood, in the form of reinforced associative learning [28]. The earliest stages of reinforced associative learning in primary sensory cortices appear to involve an active inhibition of PV inhibitory neurons via cholinergic activation of layer 1 interneurons [17,29]. Notably, our results indicate that a similar strategy – a reduction in PV cell firing rates and disinhibition of upper layer excitatory neurons – is employed during the initial stages of binocular plasticity in adolescence, though by a loss of excitatory drive onto the PV cells. Together, these observations indicate that pathways regulating cortical plasticity in the juvenile and adult cortex converge on a rapid reduction of PV cell activity.

## Methods

All in vivo recordings were conducted in accordance with procedures approved by the University of California Los Angeles Office for Protection of Research Subjects and the Chancellor's Animal Research Committee. For work using cortical slices, the Institutional Animal Care and Use Committee at the University of California, Irvine, approved all procedures. To genetically label parvalbumin-positive neurons, parvalbumin-IRES-cre knock-in female mice (Jackson Laboratories, stock#008069, generated by S Arbor, FMI) were crossed with male tdTomato reporter knock-in mice directly received from Jackson

Laboratory (Jackson Laboratories, stock #007905, 'Ai9', generated by H Zeng, Allen Brain Institute). All experimental mice were hemizygous for both transgenes (PV-Cre:Ai9). Homozygous parvalbumin-IRES-cre mice used for the above breeding were all from a F1 cross of a male and female directly received from Jackson Laboratory. Mice (male and female) were randomly assigned to either control or monocular deprivation (MD) treatment groups. Samples sizes were chosen using a target power of 0.8. In cases where analysis included a subjective component, analysis was done blind to experimental group as noted below. Monocular deprivation was performed under isoflurane/oxygen anesthesia (3% induction and 2% maintenance isoflurane), antibacterial ointment applied to eyes, lid margins trimmed and one mattress suture (silk 6-O) was used to bind the upper and lower lids. In the case of 1-day MD alert recording experiments, lid margins were not trimmed to facilitate re-opening. Any mice showing signs of eye infection or lid separation were removed from the study.

### Electrophysiological recordings in alert mice

We followed the protocol outlined in reference (30). To habituate mice to head restraint, mice were handled on the first day of training by repeatedly picking them up. On the second day, a metal bar later used to restrain the animal was fixed to the mouse's skull using dental acrylic. After a minimum of 2 days recovery, mice were placed on a floating Styrofoam ball, head fixed and allowed to run for two 10 minute sessions with a 10 minute break in between. This was repeated daily, without the 10 minute break, until mice showed signs of controlled navigation, including smooth transitions between running, walking, grooming, and balancing without motion. Typically two days of head restraint atop the spherical treadmill was sufficient. On the day of recording, a 2mm diameter craniotomy was made directly over the binocular zone of primary visual cortex. Craniotomy placement and in-vivo electrophysiology were performed as detailed in reference (31). Craniotomies were centered 3mm lateral of the sagittal suture and 1mm rostral of the lamdoid suture. All experimental animals contained neurons that were driven by both the ipsilateral and contralateral eye in the recording zone. We refer to all non-fast spiking neurons (narrow-width action potentials [2]) as excitatory pyramidal neurons, although we do not rule out the possibility that up to 10% of the neruons are inhibitory neurons. Treadmill motion was monitored by measuring intensity changes in the reflectance of a red laser beam (Keyence Corporation, part# LV-N11MN and LV-NH32) focused on the Styrofoam ball. Electrophysiological signals were acquired in cell-attached configuration using a Multiclamp 700B amplifier (Molecular Devices) in current-clamp mode, digitized (PCI-6229M, National Instruments) at a sample rate of 10 kHz and low pass filtered at 6 kHz. This method of recording is ideally suited to measuring changes in firing rates because there is not an inherent sampling bias for more active neurons, a bias that is present in other techniques that depend on isolating single units from multiunit activity

### Electrophysiological recordings in urethane anesthetized mice

We followed the protocol outlined in reference (31).

### Visual stimulation and analysis of in-vivo electrophysiology

To measure evoked firing rate at the preferred orientation, full-field drifting square wave gratings were presented at full contrast at 6 orientations spaced 30 degrees apart at two directions of motion (12 orientations), using custom software developed with Psychtoolbox in Matlab. A 40 cm-width LCD monitor was placed 25 cm directly in front of alert or urethane-anesthetized mice [31], tangent to the animal's gaze. Each stimulus was presented for 3 seconds, followed by a gray screen of equal duration. Stimulus orientations and direction were randomized. Varying spatial frequencies (0.02 and 0.04 cycles per degree) and temporal frequencies (1-2 Hz) were tested, optimal stimulation were then shown for 4-9 trials. In awake recordings, periods of grooming and any periods >60 seconds in which there was no treadmill motion detected were excluded from further analysis. Evoked rates were computed as the spike rate for a given orientation, averaged across the 3-second stimulation window and across 4-9 trials, and were baselinesubtracted. Baseline was defined as the average spike rate in response to all gray screen presentations. Evoked rate at the preferred orientation is reported. To analyze spike shape, the first 50 spike waveforms were averaged for a given cell. The 10-90% rising and falling slope, and peak (P1) and nadir (P2) amplitudes were calculated from the average trace.

### Eye shuttering

Eye shuttering was accomplished by manually placing an occluding device 5 mm in front of the eye. The occluding device was constructed of flexible light-blocking material (1.2 × 1.5 cm) mounted to a vertical post, 5 mm in diameter, coupled to a magnetic base that was released and alternately placed in front of either eye as indicated by the interleaved trial schedule.

### Visual Cortical Slice Preparations

The littermates of double transgenic mice (PV-Cre:Ai9, aged P28-P29) were used for either control or the treatment of 24 hour MD. For each experimental day, a pair of the control and MD-treated animals was deeply anesthetized using pentobarbital sodium (100 mg/kg, ip), transcardially perfused with chilled oxygenated ACSF, rapidly decapitated, and brain extracted. Coronal sections of 400 μm were cut from primary visual cortex (V1) with a vibratome (VT1200S, Leica Systems) in sucrose containing ACSF (in mM: 85 NaCl, 75 sucrose, 2.5 KCl, 25 glucose, 1.25 $NaH_2$, $PO_4$, 4 $MgCl_2$, 0.5 $CaCl_2$, and 24 $NaHCO_3$). For animals having undergone monocular deprivation, sections were taken exclusively from the hemisphere contralateral to the deprived eye. Slices were incubated for at least 30 minutes in sucrose containing ACSF at 32 °C before transferred into slice recording chambers with normal ACSF (in mM: 126 NaCl, 2.5 KCl, 26 $NaHCO_3$, 2 $CaCl_2$, 2 $MgCl_2$, 1.25 $NaH_2PO_4$, and 10 glucose). Throughout the cutting, incubation, and recording, the solutions were continuously supplied with 95% $O_2$–5% $CO_2$.

### Electrophysiology and Laser Scanning Photostimulation

Electrophysiological recordings and photostimulation were performed as in reference (32). Whole cell recordings were performed under a DIC/fluorescent Olympus microscope (BX51WI). Oxygenated ACSF at room temperature was perfused into the slice recording

chamber through a custom-designed flow system driven by pressurized 95% $O_2$–5% $CO_2$ (3 PSI) at roughly 2 mL/min. Slices were examined under a 4x objective for proper targeting of either L2/3 pyramidal neurons or tdTomato-expressing PV+ interneurons within binocular regions of mouse V1 using landmarks defined in reference ([33]). To target whole cell recordings, cells were visualized at high magnification (60X objective, 0.9 NA; LUMPlanFl/IR, Olympus). Cell bodies of recorded neurons were at least 50 μm below the surface of the slice. Patch pipettes (4 – 6 MΩresistance) made of borosilicate glass were filled with an internal solution containing (in mM) 126 K-gluconate, 4 KCl, 10 HEPES, 4 ATP-Mg, 0.3 GTP-Na, and 10 phosphocreatine (pH 7.2, 300 mOsm). Electrodes also contained 0.1% biocytin for post-hoc cell labeling and further morphological identification. Once stable whole-cell recordings were achieved with good access resistance (usually <20 MΩ), basic electrophysiological properties were examined through hyperpolarizing and depolarizing current injections. Electrophysiological data were acquired with a Multiclamp 700B amplifier (Molecular Devices), data acquisition boards (models PCI MIO 16E-4 and 6713, National Instruments), and custom modified version of Ephus software [34] (Ephus, available at https://openwiki.janelia.org/). Data were digitized at 10 kHz.

PV+ inhibitory neurons were targeted based on the red fluorescent protein (RFP) expression and verified by fast spiking patterns from current injections and large basket cell morphology. Excitatory neurons were selected based upon their pyramidal somata detected under DIC, were RFP negative, and showed adapting spiking patterns to suprathreshold intrasomatic current injections. Final cell type classification was determined by the combined characterization of RFP expression, electrophysiological and morphological properties of the recorded cells.

The laser scanning photostimulation (LSPS) procedures were similar to those described in references ([13,35]). LSPS was performed through a 4x objective lens. Stock solution of MNI-caged-I-glutamate (Tocris Bioscience) was added to 20 ml of ACSF for a concentration of 0.2 mM caged glutamate. The cortical slice image, acquired through the 4x objective, was visualized using a high-resolution digital CCD camera, and this image, in turn, was used to guide and register photostimulation sites. 2 msec duration, 20 mW pulses from a 350nm UV laser (DPSS Lasers) were delivered to the sample, controlled via an electro-optical modulator and a mechanical shutter. Focal laser spots approximated a Gaussian profile with a lateral width of 100 μm. Under our experimental conditions, LSPS evoked action potentials were recorded from stimulation locations within 124 μm (96 ± 28 μm, n = 12) of targeted somata and occurred within 150 msec post photostimulation. Synaptic currents in patched neurons were detected under voltage clamp. By systematically surveying synaptic inputs from hundreds of different sites across a large cortical region, aggregate synaptic input maps were generated for individual neurons. For our mapping experiments, a standard stimulus grid (16×16 stimulation sites, 65 $\mu m^2$ spacing) was used to tessellate V1 from pia to white matter. The LSPS site spacing was empirically determined to capture the smallest predicted distance in which photostimulation differentially activates adjacent neurons. Glutamate uncaging was delivered sequentially in a nonraster, nonrandom sequence, following a “shifting-X” pattern designed to avoid revisiting the vicinity of recently stimulated sites [36].

Because glutamate uncaging agnostically activates both excitatory and inhibitory neurons, we empirically determined the excitatory and inhibitory reversal potentials in L2/3 pyramidal cells to properly isolate EPSCs and IPSCs. In a subset of experiments, L2/3 neurons were voltage clamped at a range of holding potentials from -90mV to 5mV and GABA uncaging (0.1 mM, Invitrogen) was performed by delivering brief UV flashes (1ms, 20mW) to the perisomatic regions of targeted cells to determined the GABAergic reversal potential based upon voltage-current relationships. The average GABAergic reversal potential ranged from -69 mV to -71 mV we therefore voltage clamped the targeted pyramidal cells at -70mV to determine LSPS and spontaneously evoked EPSCs.

## Laminar Circuit Input Analysis

Photostimulation induces two forms of excitatory responses: (1) those that result from direct activation of the recorded neuron's glutamate receptors, and (2) synaptically mediated responses (EPSCs) resulting from the suprathreshold activation of presynaptic excitatory neurons. Responses that occur within 10 ms of laser pulse onset were considered direct; these responses exhibited a distinct shape and occurred immediately after glutamate uncaging. Synaptic currents with such short latencies are not possible because they would have to occur before the generation of action potentials in photostimulated neurons. Therefore, direct responses need to be excluded from local synaptic input analysis. To check for any systematic differences across treatment conditions, the spatial extent and frequency of action potentials elicited in response to direct stimulation was determined in a subset of the experiments by performing whole-cell recordings in current-clamp mode using an 8×8 mapping grid. Direct stimulation was found to be similar for control and MD; direct responses were restricted to within approximately 100 microns of the recorded soma (Control 86±22 μm n= 7 cells; MD 106±34 μm n= 5 cells) and were limited to less than 1.5 action potentials averaged across trials (Control 1±0 n=7 cells; MD 1.2±0.2 n=5 cells). At some locations, synaptic responses were over-riding on relatively small direct responses (cf. Fig. S1d); such responses were identified and included in synaptic input analysis.

For data map analysis, we implemented the approach for detection and extraction of photostimulation-evoked postsynaptic current responses described in reference (37). LSPS evoked EPSCs were quantified across the 16×16 mapping grid for each cell, and 2 to 4 individual maps were averaged per recorded cell, reducing the likelihood of incorporating noise events in the analysis window (150 msec). Averaged maps were then analyzed using the 4X DIC image to bin responses according to laminar cytoarchitectonic landmarks. Synaptic events were binned from locations spanning ± 195 μm tangential to the targeted soma location and from the top of layer 2/3 to the bottom of layer 6 across the radial vector. Data were plotted as either the average integrated EPSCs amplitude per pixel location or the number of EPSCs detected per pixel location.

## Morphological examination and Cell-type Identification

The morphology of each recorded neuron was determined using post-hoc staining. Briefly, brain slices were fixed in 4% paraformaldehyde and transferred to 30% sucrose solution in phosphate buffered saline (PBS). Neurons filled with biocytin during recordings were labeled with Alexa Fluor 488 -conjugated streptavidin (1:500 dilution; Jackson

ImmunoResearch). Slices were also stained for 4′-6-diamidino-2-phenylindole (DAPI) (Sigma-Aldrich) to identify laminar boundaries. Cell morphology, DAPI labeling, and RFP expression were visualized using an Olympus BX 61 epifluorescent microscope and MetaMorph imaging suite (Molecular Devices).

### Calcium Imaging using Oregon Green BAPTA-1

Mice were anesthetized with urethane and core body temperature was maintained using a closed loop heated plate and a rectal temperature sensor. Neurons in layer 2/3 of primary visual cortex were bulk labeled with the calcium indicator Oregon Green BAPTA-1, and changes in fluorescence intensity were imaged as described in references (38,39). Dye was injected at 2-3 positions to ensure labeling within the binocular region. Three days prior to calcium imaging, mice were randomly assigned to one of three groups: control, MD, or MD + diazepam (DZ; pharmaceutical grade, Hospira) treatment. Intraventricular injections (1.5 μL volume) of either vehicle (50% propylene glycol/ 50% saline) or DZ (2mg/ml in 50% propylene glycol) were performed in isoflurane/oxygen anesthetized mice (3% induction, 1-2% maintenance) using a Hamilton needle (30 gauge) and syringe (5 μL capacity) mounted to a manipulator (MP285, Sutter). The injection depth was 2.25 mm; entry site was 0.5 mm lateral from midline and immediately anterior of bregma (primary motor cortex). Two injections were made, the initial injection was made at the time of MD on the same side as the MD, and the second injection was made on the other hemisphere 24-28 hours following the initial injection. Coordinates were verified prior to the experiment in 3 test animals by injecting DiI (0.5 μL) and perfusing mice 1 day later. Brains were then sectioned, slices were visualized under epifluorescence and it was determined that DiI was specifically localized to ventricles using the above coordinates.

### Expression of GCaMP6 and hM4D DREADD receptors

PV-Cre mice were anesthetized with isoflurane and core body temperature maintained as above. The scalp was retracted and a small burr hole was drilled over the left occipital pole overlying the binocular zone of primary visual cortex. GCaMP6 (Chen et al., Nature 2013, in press; UPenn Vector Core: AAV-1-PV2824; generously supplied by the GENIE Project, Janelia Farm Research Campus, HHMI) and Cre-dependent hM4D DREADD receptors [19,20,40] (UNC Vector Core: AAV-hSyn-DIO-hM4D(Gi)-mCherry) were expressed in cortical neurons using adeno-associated virus (AAV). Notably, hM4D receptors were only expressed in PV-Cre cells. AAV-GCaMP6 and AAV-hM4D were mixed at a 1:1 ratio (injected concentration 2.5e11 genome copies/mL) and loaded into a glass micropipette. The pipette was slowly inserted into the cortex and 5 injections were made, 1 each at 350, 300, 250, 200, and 150 micrometers below the pial surface along a single injection tract. AAV was pressure injected at each site using a Picospritzer: 30 puffs at 10psi and 10msec duration were used at each site. Total volume injected across all 5 sites was roughly 0.5 microliters. The scalp was then sutured shut over the burr hole and the mouse was left for 2 weeks to enable high GCaMP6 and hM4D expression. Thereafter, a craniotomy was performed to expose a 2.5mm diameter region of the brain centered on binocular visual cortex, and the craniotomy was sealed with a No. 1 coverglass as described previously [41].

## Visual stimulation and data acquisition

To evoke responses in labeled neurons, visual stimuli were presented based on the methods of reference (42). Neural responses to stimulation of either eye were assessed using full-field drifting square wave gratings presented at full contrast at 6 orientations spaced 30 degrees apart at two directions of motion (12 orientations, temporal frequency of 2 Hz, 0.04 cycles/degree) every 11 seconds for a duration of 5 seconds preceded by a gray screen for a duration of 6 seconds. During the stimulation time, randomly chosen grating orientations changed every 0.4 seconds. Four stimulus repetitions were presented and interleaved between eye stimulation. Image sequences (256×256 pixels, covering a field of view of 130×130 microns) were acquired at 2.05 Hz at a depth of 180 – 300 microns below the pia surface using ScanImage software [43]. Fields of view that contained no or unevenly distributed responses to ipsilateral eye stimulation, an indication that the imaged position was outside or at the border of the binocular zone, were excluded from further analysis. Neurons were distinguished from astrocytes using sulforhodamine coinjection [44]. During OGB and GCaMP6 imaging, red (Semrock filter: 583/22) and green (Semrock filter: 510/84) emissions were separated (Semrock dichroic: FF568) and detected simultaneously using two photomultiplier tubes (PMTs; Hamamatsu R3896). OGB was excited at wavelength of 870 nm. GCaMP6 was excited at 940nm. When imaging OGB, PV interneurons were subsequently identified and excluded from analysis by switching the excitation wavelength to 960 nm. When imaging GCaMP6, PV interneurons were identified by their emission in the red channel. To facilitate defining the stimulus onset for each cell, output from a photodiode affixed to the presentation monitor was digitized simultaneously with the output from the PMTs.

For GCaMP6/hM4D expressing mice, images of cell responses to visual stimulation were first obtained on P35. Immediately thereafter the lid margins to the contralateral eye were sutured shut for 3 days. During the first day of lid suture mice either received two I.P. injections, spaced 12 hours apart of either saline or clozapine-N-oxide (CNO) (5mg/Kg dissolved in 0.9% sterile saline). On P38, the lid margins were re-opened and cortical responses to visual stimulation through both the ipsilateral and contralateral eyes were assessed. Distributions of ipsilateral and contralateral response strength after MD in both conditions were compared to those obtained from baseline images.

## Data Analysis

A semiautomatic custom-written routine (Matlab) was used to identify the outlines of individual OGB-loaded cells [38]. Briefly, an average image was generated from the acquired time series and the x,y spatial position of a given cell was seeded by the user, blind to experimental condition. The spatial location of the cell border was then calculated based on identifying a contiguous region having a >1.1-fold intensity above the local average. Local average and maximum cell size was bounded by a square area R × R centered on the user defined seed pixel, where R= 25 microns. For GCaMP6 imaging, where labeled neurons have a donut appearance, we used a separate method for segmenting neurons. In brief, after manual selection of the cells to be studied, a deformable snake was used to track their individual boundaries [45], along with morphological dilation [46] to define the region of interest for each cell. For both OGB and GCaMP6 images, the pixels within each cell's

region of interest were averaged to generate a single time course of fluorescent intensity for each individual cell. Response amplitude was computed from 8-12 stimulus repetitions as the first 5 frames immediately following the frame of stimulus onset divided by the average of the 6 frames preceding stimulus onset. The frame of stimulus onset was defined independently for each cell. Cells were considered responsive if the calcium transients to any of the orientation stimuli were significantly different from the baseline (ANOVA at $p<0.01$). An OD score was calculated for all responsive cells (excluding identified PV interneurons and astrocytes) as 1 minus the ratio of the ipsilateral eye response divided by the summed response of both eyes. For each animal, a histogram of OD scores was generated and the contralateral bias index was calculated as in ref [9], using the following formula: $( (n_1-n_7)+(2/3)*(n_2-n_6)+(1/3)*(n_3-n_5) +N ) / (2*N)$, where N=total number of responsive cells and $n_x$ is the number of cells with OD scores equal to x.

### Statistical analyses and bar graphs

All data are reported as mean ± standard error of the mean (SEM). When comparing two independent groups, normally distributed data were analyzed using a student's t-test, in the case data were not normally distributed a Mann-Whitney U test was used. In the case more than 2 groups were compared and data were normally distributed, an ANOVA was performed as indicated in main text and followed by post-hoc comparisons when justified (alpha set to 0.05). Post-hoc P values were corrected for multiple comparisons as indicated. Bonferroni correction was used unless data had unequal variances (assessed by the Levene Statitistic), in that case Tamhane correction was used. In all cases, sample size n was defined as cell number, except in the case of comparing the contralateral bias index across treatments and GCaMP6 'optical field potential'; n was defined as animal number.

## Supplementary Material

Refer to Web version on PubMed Central for supplementary material.

## Acknowledgments

We thank S. Smith, W. Thompson, K. Miller, and M.P. Stryker for comments on earlier versions of this manuscript, Y.Shi for help with software, Z.Nenadic for analytical suggestions, D. Ringach for help with GCaMP6 analysis, and Z.J Huang for useful discussions. This work was funded by grants from the US National Eye Institute (EY016052) to JTT and and the US National Institute of Neurological Disorders and Stroke (NS078434) to XX.

## References

1. Ko H, et al. The emergence of functional microcircuits in visual cortex. Nature. 2013; 496:96–100. [PubMed: 23552948]
2. White LE, Fitzpatrick D. Vision and cortical map development. Neuron. 2007; 56:327–338. [PubMed: 17964249]
3. Wiesel TN, Hubel DH. Single-Cell Responses in Striate Cortex of Kittens Deprived of Vision in One Eye. J Neurophysiol. 1963; 26:1003–1017. [PubMed: 14084161]
4. Levelt CN, Hubener M. Critical-period plasticity in the visual cortex. Annu Rev Neurosci. 2012; 35:309–330. [PubMed: 22462544]
5. Hensch TK. Critical period plasticity in local cortical circuits. Nat Rev Neurosci. 2005; 6:877–888. [PubMed: 16261181]

6. Jiang B, Huang ZJ, Morales B, Kirkwood A. Maturation of GABAergic transmission and the timing of plasticity in visual cortex. Brain Res Brain Res Rev. 2005; 50:126–133. [PubMed: 16024085]
7. Fu M, Zuo Y. Experience-dependent structural plasticity in the cortex. Trends Neurosci. 2011; 34:177–187. [PubMed: 21397343]
8. Holtmaat A, Svoboda K. Experience-dependent structural synaptic plasticity in the mammalian brain. Nat Rev Neurosci. 2009; 10:647–658. [PubMed: 19693029]
9. Gordon JA, Stryker MP. Experience-dependent plasticity of binocular responses in the primary visual cortex of the mouse. J Neurosci. 1996; 16:3274–3286. [PubMed: 8627365]
10. Webber AL, Wood J. Amblyopia: prevalence, natural history, functional effects and treatment. Clin Exp Optom. 2005; 88:365–375. [PubMed: 16329744]
11. Holmes JM, et al. Effect of Age on Response to Amblyopia Treatment in Children. Arch Ophthalmol. 2011
12. Kanonidou E. Amblyopia: a mini review of the literature. International ophthalmology. 2011; 31:249–256. [PubMed: 21424553]
13. Shepherd GM, Svoboda K. Laminar and columnar organization of ascending excitatory projections to layer 2/3 pyramidal neurons in rat barrel cortex. J Neurosci. 2005; 25:5670–5679. [PubMed: 15958733]
14. Yoshimura Y, Callaway EM. Fine-scale specificity of cortical networks depends on inhibitory cell type and connectivity. Nat Neurosci. 2005; 8:1552–1559. [PubMed: 16222228]
15. Weiler N, Wood L, Yu J, Solla SA, Shepherd GM. Top-down laminar organization of the excitatory network in motor cortex. Nat Neurosci. 2008; 11:360–366. [PubMed: 18246064]
16. Lambo ME, Turrigiano GG. Synaptic and Intrinsic Homeostatic Mechanisms Cooperate to Increase L2/3 Pyramidal Neuron Excitability during a Late Phase of Critical Period Plasticity. J Neurosci. 2013; 33:8810–8819. [PubMed: 23678123]
17. Letzkus JJ, et al. A disinhibitory microcircuit for associative fear learning in the auditory cortex. Nature. 2011; 480:331–335. [PubMed: 22158104]
18. Harauzov A, et al. Reducing intracortical inhibition in the adult visual cortex promotes ocular dominance plasticity. J Neurosci. 2010; 30:361–371. [PubMed: 20053917]
19. Ferguson SM, et al. Transient neuronal inhibition reveals opposing roles of indirect and direct pathways in sensitization. Nat Neurosci. 2011; 14:22–24. [PubMed: 21131952]
20. Armbruster BN, Li X, Pausch MH, Herlitze S, Roth BL. Evolving the lock to fit the key to create a family of G protein-coupled receptors potently activated by an inert ligand. Proc Natl Acad Sci U S A. 2007; 104:5163–5168. [PubMed: 17360345]
21. Dong S, Allen JA, Farrell M, Roth BL. A chemical-genetic approach for precise spatio-temporal control of cellular signaling. Molecular bioSystems. 2010; 6:1376–1380. [PubMed: 20532295]
22. Li H, et al. Experience-dependent modification of a central amygdala fear circuit. Nat Neurosci. 2013; 16:332–339. [PubMed: 23354330]
23. Alexander GM, et al. Remote control of neuronal activity in transgenic mice expressing evolved G protein-coupled receptors. Neuron. 2009; 63:27–39. [PubMed: 19607790]
24. Chen T-W, et al. Ultrasensitive fluorescent proteins for imaging neuronal activity. Nature. 2013
25. Kameyama K, et al. Difference in binocularity and ocular dominance plasticity between GABAergic and excitatory cortical neurons. J Neurosci. 2010; 30:1551–1559. [PubMed: 20107082]
26. Gandhi SP, Yanagawa Y, Stryker MP. Delayed plasticity of inhibitory neurons in developing visual cortex. Proc Natl Acad Sci U S A. 2008; 105:16797–16802. [PubMed: 18940923]
27. Yazaki-Sugiyama Y, Kang S, Cateau H, Fukai T, Hensch TK. Bidirectional plasticity in fast-spiking GABA circuits by visual experience. Nature. 2009; 462:218–221. [PubMed: 19907494]
28. de Villers-Sidani E, Merzenich MM. Lifelong plasticity in the rat auditory cortex: basic mechanisms and role of sensory experience. Prog Brain Res. 2011; 191:119–131. [PubMed: 21741548]
29. Froemke RC, Merzenich MM, Schreiner CE. A synaptic memory trace for cortical receptive field plasticity. Nature. 2007; 450:425–429. [PubMed: 18004384]

30. Dombeck DA, Khabbaz AN, Collman F, Adelman TL, Tank DW. Imaging large-scale neural activity with cellular resolution in awake, mobile mice. Neuron. 2007; 56:43–57. [PubMed: 17920014]
31. Kuhlman SJ, Tring E, Trachtenberg JT. Fast-spiking interneurons have an initial orientation bias that is lost with vision. Nat Neurosci. 2011; 14:1121–1123. [PubMed: 21750548]
32. Xu X, Olivas ND, Levi R, Ikrar T, Nenadic Z. High precision and fast functional mapping of cortical circuitry through a novel combination of voltage sensitive dye imaging and laser scanning photostimulation. J Neurophysiol. 2010; 103:2301–2312. [PubMed: 20130040]
33. Antonini A, Fagiolini M, Stryker MP. Anatomical correlates of functional plasticity in mouse visual cortex. J Neurosci. 1999; 19:4388–4406. [PubMed: 10341241]
34. Suter BA, et al. Ephus: multipurpose data acquisition software for neuroscience experiments. Front Neural Circuits. 2010; 4100
35. Hooks BM, et al. Laminar analysis of excitatory local circuits in vibrissal motor and sensory cortical areas. PLoS Biol. 2011; 9:e1000572. [PubMed: 21245906]
36. Shepherd GM, Pologruto TA, Svoboda K. Circuit analysis of experience-dependent plasticity in the developing rat barrel cortex. Neuron. 2003; 38:277–289. [PubMed: 12718861]
37. Shi Y, Nenadic Z, Xu X. Novel use of matched filtering for synaptic event detection and extraction. PLoS ONE. 2010; 5:e15517. [PubMed: 21124805]
38. Gdalyahu A, et al. Associative fear learning enhances sparse network coding in primary sensory cortex. Neuron. 2012; 75:121–132. [PubMed: 22794266]
39. Stosiek C, Garaschuk O, Holthoff K, Konnerth A. In vivo two-photon calcium imaging of neuronal networks. Proc Natl Acad Sci U S A. 2003; 100:7319–7324. [PubMed: 12777621]
40. Rogan SC, Roth BL. Remote control of neuronal signaling. Pharmacological reviews. 2011; 63:291–315. [PubMed: 21415127]
41. Holtmaat A, et al. Long-term, high-resolution imaging in the mouse neocortex through a chronic cranial window. Nat Protoc. 2009; 4:1128–1144. [PubMed: 19617885]
42. Mrsic-Flogel TD, et al. Homeostatic regulation of eye-specific responses in visual cortex during ocular dominance plasticity. Neuron. 2007; 54:961–972. [PubMed: 17582335]
43. Pologruto TA, Sabatini BL, Svoboda K. ScanImage: flexible software for operating laser scanning microscopes. Biomed Eng Online. 2003; 2:13. [PubMed: 12801419]
44. Nimmerjahn A, Kirchhoff F, Kerr JN, Helmchen F. Sulforhodamine 101 as a specific marker of astroglia in the neocortex in vivo. Nat Methods. 2004; 1:31–37. [PubMed: 15782150]
45. Xu C, Prince JL. Snakes, shapes, and gradient vector flow. IEEE transactions on image processing : a publication of the IEEE Signal Processing Society. 1998; 7:359–369. [PubMed: 18276256]
46. Serra, J.; Soille, P. Mathematical morphology and its applications to image processing (Computational Imaging and Vision). Springer; 1994.

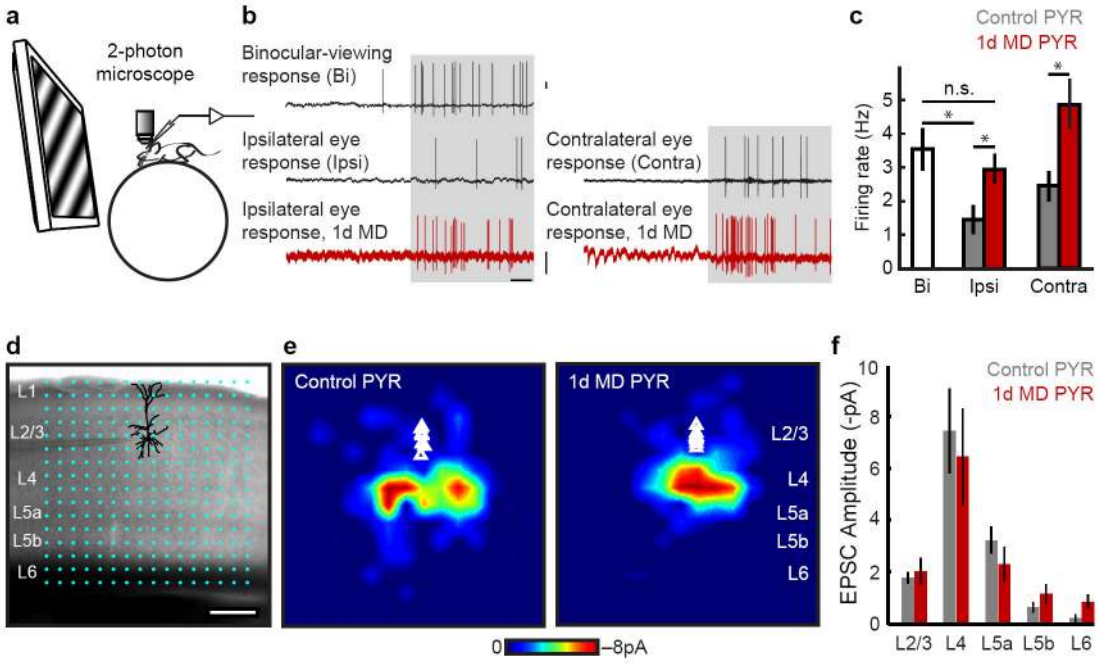


**Figure 1. L2/3 pyramidal neuron responsiveness and local circuit organization is unchanged 1d after MD**

**a-c**, Responses of pyramidal (PYR) neurons to drifting gratings in alert mice. **a**, Cartoon of head-fixed configuration. **b**, Example loose-cell attached recordings from controls (black) and after 1d MD (red) in response to visual stimulation (gray shading). Scale: 1mV, 500 ms. **c**, Mean firing rate at optimal orientation (Bi 10 mice, *n*= 30 cells; Ipsi control 7 mice, *n*= 22 cells; Ipsi MD 6 mice, *n*= 33 cells; Contra control 3 mice, *n*= 9 cells; Contra MD 3 mice, *n*= 10 cells). **d**, PYR neuron recorded in binocular V1 in an acute slice; overlaid are 16 ×16 LSPS stimulation locations spanning pia to white matter. **e**, In vitro LSPS aggregate excitatory input maps pooled across PYR neurons, triangles indicate soma location (Control 4 mice, *n*= 9 cells; MD 4 mice, *n*= 9 cells). Scale: 200 μm. **f**, Mean LSPS-evoked EPSC amplitude, same cells as e. *P<0.05.

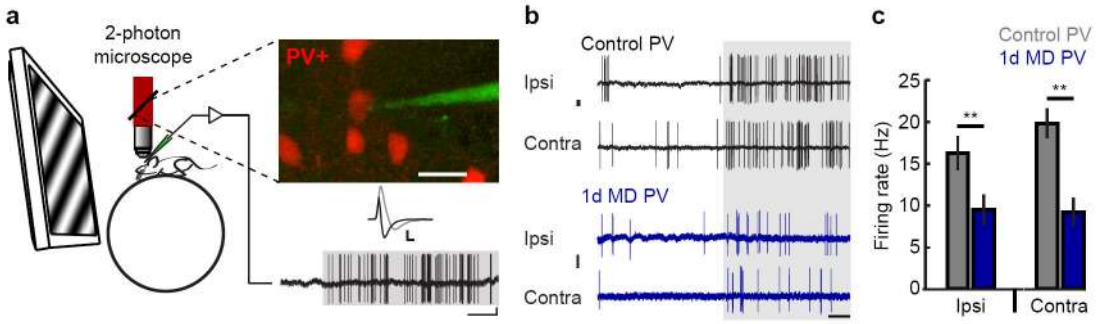


**Figure 2. L2/3 PV responsiveness to visual stimuli is reduced after 1d MD**

**a**, Cartoon of targeted recording in alert mice (left). Two-photon excitation (red beam) is used to visualize PV cells expressing tdTomato and recording pipette filled with Alexa dye (inset, 6 red PV cells, the pipette, green, is loose cell-attached to the PV cell in the center of the image; scale: 20 μm). Spike waveform is used to verify targeting of fast-spiking PV cells (black trace; gray trace is a PYR neuron waveform for comparison, scale: 0.5 mV, 1 ms). Bottom, example PV response to visual stimulation (gray shading, scale: 1mV, 500 ms). **b**, Example PV responses evoked by stimulation through either eye in control (black) and 1d MD (blue) anesthetized mice. Scale bar: 1mV, 500 ms. **c**, Mean firing rate at optimal orientation (Ipsi control 14 mice, *n*= 26 cells; Ipsi MD 5 mice, *n*= 18 cells; Contra control 14 mice, *n*= 26 cells; Contra MD 5 mice, *n*= 18 cells). ** P<0.005

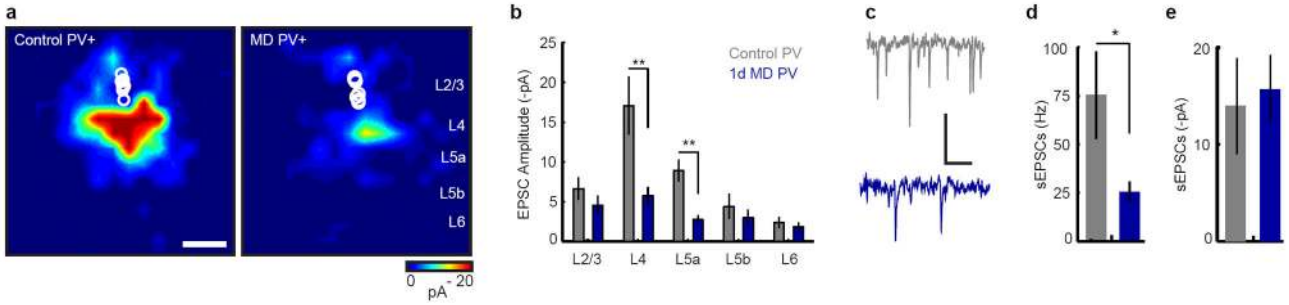


**Figure 3. L2/3 PV local circuit organization is altered after 1d MD**

**a**, In vitro LSPS aggregate excitatory input maps pooled across PV cells, circles indicate soma location (Control 4 mice, *n*= 7 cells; MD 4 mice, *n*= 7 cells). Scale: 200 μm. **b**, Mean laminar LSPS-evoked EPSC amplitude, same cells as a. **P<0.007. **c**, Example sEPSCs, scale: 20 pA, 100 ms. **d**, Mean sEPSC frequencies, same cells as a. *P<0.05 **e**, Mean sEPSC amplitude, same cells as a.

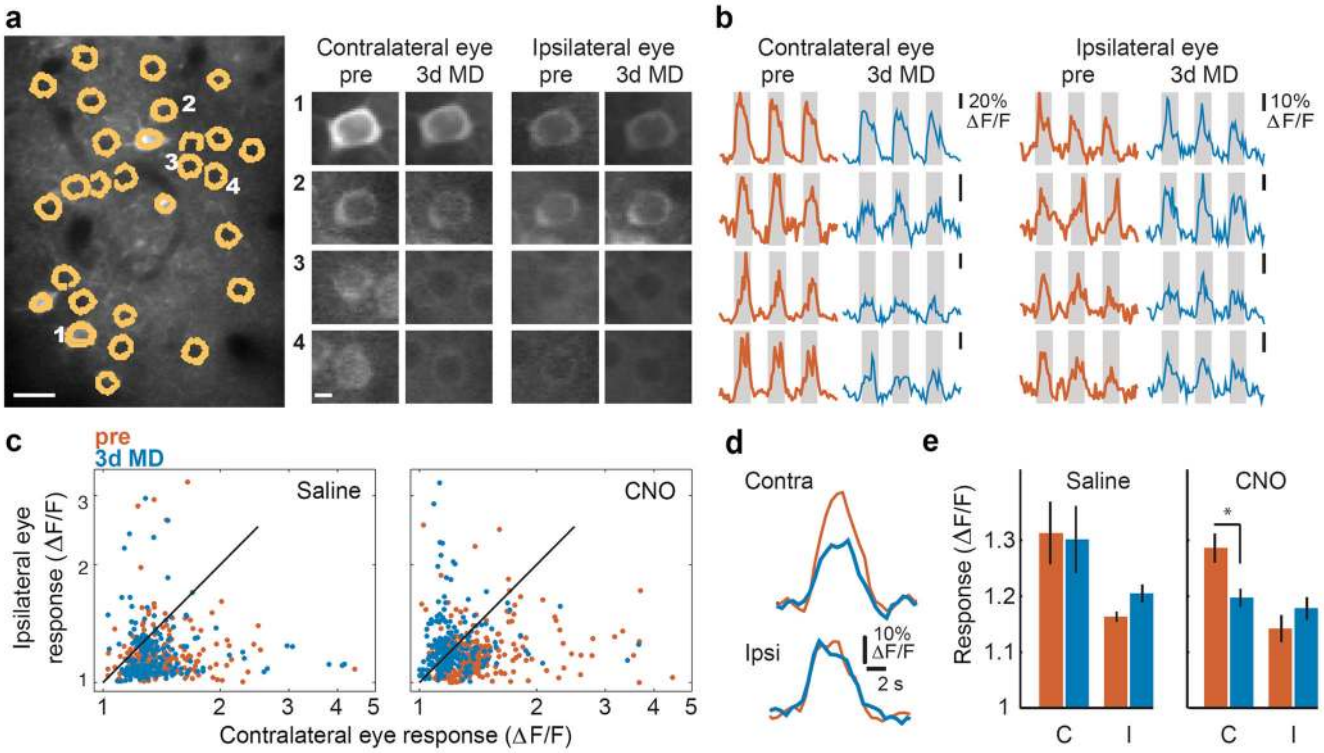


**Figure 4. Reducing PV-specific inhibition restores ocular dominance plasticity after the closure of the critical period**

**a**, *In vivo* image of GCaMP6 expression, cells outlined in yellow, scale: 20μm. Right, individual cell images (1-4) of the average evoked fluorescence in response to visual stimuli presented independently to the contralateral and ipsilateral eye, before (Pre) and 3 days after MD in a mouse expressing the hM4D DREADD receptor specifically in PV cells, treated with CNO; scale: 5 μm. **b**, Relative change in fluorescence before and after 3d MD + CNO for cells 1-4 in panel a in response to visual stimulation (gray shading; 5s duration). **c**, Log-log scatter plot of visually evoked fluorescence response for each cell (saline *n*= 242 cells; CNO *n*= 327 cells). Note the significant leftward shift after 3d MD in mice treated with CNO, but not those treated with saline, indicating a reduced response to contralateral eye stimulation after 3d MD. **d**, Longitudinal 'optical field potential' response (average value of all pixels in the entire imaging field, inclusive of neuropil) for the region in panel a. Note the decrease in response to contralateral eye stimulation after MD + CNO that is not seen for the ipsilateral eye. **e**, Mean 'optical field potential' response (Saline *n*= 4 mice; CNO *n*=4 mice). * P<0.05.